Neuron 49, 107–117, January 5, 2006 ©2006 Elsevier Inc. DOI 10.1016/j.neuron.2005.11.036

Shunting Inhibition Improves Robustness of Gamma Oscillations in Hippocampal Interneuron Networks by Homogenizing Firing Rates

Imre Vida,[1,3] Marlene Bartos,[2,3] and Peter Jonas[2,*]
[1] Anatomisches Institut
Universität Freiburg
Albertstr. 17
D-79104 Freiburg
Germany
[2] Physiologisches Institut
Universität Freiburg
Hermann-Herder-Str. 7
D-79104 Freiburg
Germany

Summary

Networks of GABAergic neurons are key elements in the generation of γ oscillations in the brain. Computational studies suggested that the emergence of coherent oscillations requires hyperpolarizing inhibition. Here, we show that $GABA_A$ receptor-mediated inhibition in mature interneurons of the hippocampal dentate gyrus is shunting rather than hyperpolarizing. Unexpectedly, when shunting inhibition is incorporated into a structured interneuron network model with fast and strong synapses, coherent oscillations emerge. In comparison to hyperpolarizing inhibition, networks with shunting inhibition show several advantages. First, oscillations are generated with smaller tonic excitatory drive. Second, network frequencies are tuned to the γ band. Finally, robustness against heterogeneity in the excitatory drive is markedly improved. In single interneurons, shunting inhibition shortens the interspike interval for low levels of drive but prolongs it for high levels, leading to homogenization of neuronal firing rates. Thus, shunting inhibition may confer increased robustness to γ oscillations in the brain.

Introduction

Gamma frequency oscillations (30–90 Hz) are thought to be of critical importance for information processing in neuronal networks (Singer, 1999; Traub et al., 1999; Salinas and Sejnowski, 2001; Buzsáki and Draguhn, 2004). These oscillations may serve as reference signals for temporal encoding of information in neuronal ensembles (Singer, 1999; Buzsáki and Draguhn, 2004) and could also enhance plasticity at glutamatergic synapses by synchronizing action-potential firing in pre- and postsynaptic neurons (Dan and Poo, 2004). In the hippocampus, γ oscillations are assumed to underlie the encoding of spatial information and the formation of episodic memory (Lisman, 1999). Several lines of evidence suggest that networks of mutually connected GABAergic interneurons play a key role in the generation of γ oscillations. Most importantly, pharmacologically isolated interneuron networks can generate γ activity in the presence of a tonic excitatory drive in vitro (Whittington et al., 1995; Towers et al., 2002; Fisahn et al., 2004). Furthermore, interneurons, in particular fast-spiking basket cells (BCs), fire high-frequency bursts of action potentials tightly phase locked to γ oscillations both in vitro (Hájos et al., 2004; Gloveli et al., 2005) and in vivo (Bragin et al., 1995; Penttonen et al., 1998; Csicsvari et al., 2003).

Although the primary role of interneurons in the generation of network oscillations is well established, the underlying mechanisms are less well understood. Computational studies showed that interneuron network models generate coherent activity in the γ frequency band in response to a tonic excitatory drive (Traub et al., 1996; Wang and Buzsáki, 1996; Bartos et al., 2002). The basic principle of synchronization is as follows: if a sufficiently large population of neurons fires within a short time interval, it generates a synchronized inhibitory synaptic conductance in the network. Neurons will escape from inhibition jointly and fire subsequent action potentials at the same time, leading to synchronized activity. If connectivity is high and synapses are sufficiently strong, synchronization in a small ensemble of neurons can rapidly lead to synchronization of the entire network (Bartos et al., 2002). For efficient synchronization, inhibition is generally assumed to be hyperpolarizing (Wang and Rinzel, 1992; van Vreeswijk et al., 1994; Traub et al., 1996; Wang and Buzsáki, 1996; Bartos et al., 2002).

A consistent problem of interneuron network models is the requirement for a highly homogeneous tonic excitatory drive. If the drive is heterogeneous, the intrinsic action-potential frequency of individual neurons will also be heterogeneous, and global synchrony cannot be maintained (Ermentrout and Kopell, 1990; Wang and Buzsáki, 1996; White et al., 1998; Tiesinga and José, 2000; Kopell and Ermentrout, 2004). In networks with slow and weak synapses, coherent oscillations break down if the heterogeneity in the tonic drive exceeds 3% (Wang and Buzsáki, 1996). Robustness against heterogeneity can be improved by incorporating fast and strong synapses (Neltner et al., 2000; Bartos et al., 2001, 2002; Kopell and Ermentrout, 2004). Under these conditions, coherent oscillations can be generated with heterogeneity levels up to 10% (Bartos et al., 2001). However, a large amplitude of the excitatory drive is needed to counterbalance the increased level of inhibition under these conditions (Neltner et al., 2000). The requirements for large amplitude and small heterogeneity of the tonic excitatory drive are inconsistent with experimental data. Although activation of both metabotropic glutamate receptors (mGluRs) and kainate receptors efficiently induces γ oscillations in vitro (Whittington et al., 1995; Fisahn et al., 2004), the corresponding tonic excitatory currents in interneurons are small and highly variable (coefficient of variation ~35% for mGluR responses in fast-spiking CA1 interneurons [van Hooft et al., 2000]; ~53% for kainate responses in CA3 interneurons [Fisahn et al., 2004]; see Parra et al. [1998]).

How can these discrepancies between experiments and models be reconciled? One possibility to reduce

*Correspondence: peter.jonas@physiologie.uni-freiburg.de
[3] These authors contributed equally to this work.

the requirement for a large excitatory drive would be to shift the synaptic reversal potential (E_{syn}) to more depolarized values. If inhibition was shunting or depolarizing rather than hyperpolarizing, as suggested by recent experimental data in interneurons of the amygdala and the cerebellum (Martina et al., 2001; Chavas and Marty, 2003), a smaller drive may be sufficient to excite the neurons in the network and to generate coherent activity, as proposed for slow sleep spindle oscillations in thalamic networks (Bazhenov et al., 1999). However, simulations of fast oscillations in interneuron network models demonstrated that coherence breaks down steeply as E_{syn} is shifted from hyperpolarizing into shunting or depolarizing regimes (Wang and Buzsáki, 1996). Thus, it is widely believed that hyperpolarizing inhibition is required for the emergence of coherent oscillations in interneuron networks (Wang and Rinzel, 1992; van Vreeswijk et al., 1994; Wang and Buzsáki, 1996).

To examine the relation between synaptic reversal potential and synchronization, we pursued a three-step strategy. First, we measured E_{syn} of $GABA_A$ receptor-mediated inhibition in fast-spiking BCs by noninvasive gramicidin-perforated patch recording. Second, we analyzed the impact of E_{syn} on coherence and frequency of γ oscillations in interneuron network models with realistic synapses (Bartos et al., 2002; Galarreta and Hestrin, 2002). Finally, we examined the effects of different forms of inhibition on the timing of action potentials in a single-cell model and in hippocampal BCs with a dynamic clamp. We find that the synaptic reversal potential in hippocampal BCs is between the resting potential and action-potential threshold (Fricker et al., 1999). In the following, we will refer to this form of inhibition as "shunting" (Alger and Nicoll, 1979; Andersen et al., 1980). Unexpectedly, shunting inhibition not only supports the generation of coherent γ activity but greatly increases the robustness against heterogeneities by homogenizing the firing rates of weakly and strongly excited neurons.

Results

$GABA_A$ Receptor-Mediated Inhibition in Fast-Spiking Basket Cells Is Shunting

We examined the reversal potential of $GABA_A$ receptor-mediated inhibitory postsynaptic currents (IPSCs) in BCs of the dentate gyrus in rat and mouse hippocampal slices (Figure 1). To preserve the intracellular Cl^- concentration, we made recordings in the perforated-patch configuration with the ionophore gramicidin D (Figure 1A) (Kyrozis and Reichling, 1995). Synaptic events were evoked by extracellular axon stimulation, and IPSCs were isolated pharmacologically (Figure 1B). Bath application of 20 μM bicuculline blocked IPSCs under these conditions, confirming that they were mediated by $GABA_A$ receptors (four of four cells). To determine E_{syn}, we recorded IPSCs at incremental holding potentials, and analyzed current-voltage relations by polynomial fitting (Figures 1B and 1C). For BCs in rats and BCs in transgenic mice labeled by the expression of green fluorescent protein under the control of the parvalbumin promoter (PV-BCs), E_{syn} was -52.3 ± 1.9 mV (seven cells) and -52.0 ± 2.7 mV (three cells), respectively (Figure 1D). Comparison of synaptic reversal potentials with the resting potentials of the same cells revealed that E_{syn} was significantly more positive than the resting potential in BCs and PV-BCs (-58.4 ± 1.4 mV and -59.3 ± 1.9 mV, respectively; $p < 0.05$; Figures 1D and 1E). Thus, inhibition in these cells is shunting (Chavas and Marty, 2003) rather than hyperpolarizing (Lamsa and Taira, 2003).

Shunting Inhibition Supports Gamma Oscillations in Interneuron Networks

To address whether shunting inhibition supports the generation of γ oscillations in interneuron networks, we examined the activity of an experimentally constrained model of fast-spiking BCs interconnected by fast and strong synapses (Bartos et al., 2002; Galarreta and Hestrin, 2002) (Figure 2). Two values of E_{syn} were compared, -75 mV, as assumed in previous simulations, and -55 mV, as suggested by our experimental findings. The network was activated by a low tonic excitatory drive ($I_\mu = 0.5\ \mu A\ cm^{-2}$) with moderate cell-to-cell heterogeneity ($I_\sigma / I_\mu = 10\%$, in which I_σ is the standard deviation and I_μ is the mean of the amplitudes of the tonic drive). When E_{syn} was -75 mV, the network oscillated with low coherence at low frequency (20 Hz, corresponding to the β band; Figure 2B). Unexpectedly, when E_{syn} was -55 mV, the network oscillated with markedly increased coherence and with higher frequency (85 Hz, corresponding to the upper γ band; Figure 2C).

We further examined the relation between network frequency (f), coherence (κ), and E_{syn} (Figures 2D and 2E). Two regimes were considered: a hyperpolarizing regime with E_{syn} < resting membrane potential (*rmp*) and a shunting regime with $rmp \leq E_{syn}$ < action-potential threshold (*thres*). A third regime with $E_{syn} \geq thres$ was not considered because the synaptic conductance would be purely excitatory in this scenario. When E_{syn} was varied from -80 to -45 mV for a constant drive of $0.5\ \mu A\ cm^{-2}$, network frequency (f) increased monotonically (Figure 2D). Coherence (κ), as quantified by a cross-correlation-based measure, showed a maximum for an E_{syn} of -55 mV but declined for more depolarized and hyperpolarized potentials (Figure 2E). Finally, the proportion of active cells was close to 100% with shunting inhibition, whereas it was significantly smaller for hyperpolarizing inhibition where the highly excited cells silenced the weakly excited cells (Figure 2F) (Kopell and Ermentrout, 2004). Thus, contrary to our expectations, shunting inhibition supports the generation of coherent γ activity and minimizes suppression in interneuron networks with fast and strong synapses.

Coherence and frequency of network oscillations are critically dependent on the amplitude of the tonic excitatory drive (I_μ) and the unitary inhibitory conductance (g_{syn}) (Traub et al., 1996; Wang and Buzsáki, 1996; Bartos et al., 2002). However, both I_μ and g_{syn} are variable (Parra et al., 1998; van Hooft et al., 2000; Fisahn et al., 2004; Bartos et al., 2001, 2002; Galarreta and Hestrin, 2002). We therefore analyzed the dependence of coherence and frequency on I_μ and g_{syn} for both hyperpolarizing and shunting inhibition (Figure 3). With a moderate cell-to-cell heterogeneity ($I_\sigma / I_\mu = 10\%$), the network based on hyperpolarizing inhibition generated coherent oscillations within a subregion of the parameter space (Figure 3A) (see Bartos et al. [2002]). Frequencies

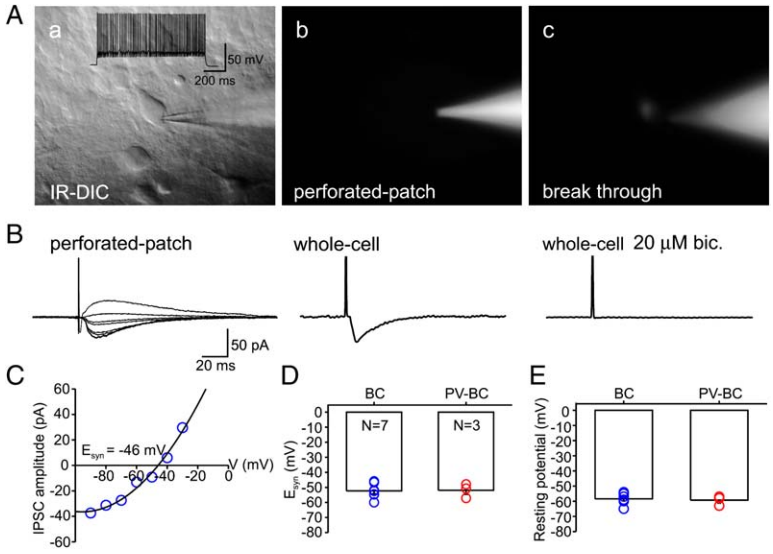

Figure 1. Inhibition Is Shunting in Fast-Spiking Dentate Gyrus BCs

(A) Gramicidin D perforated-patch recordings from a BC. (Aa) IR-DIC image of the BC soma located at the border between granule cell layer and hilus in rat hippocampal slice. Inset shows fast-spiking action-potential phenotype. (Ab) Epifluorescence image of the same cell to monitor the stability of the recording. Note that Alexa 594 is restricted to the recording pipette, indicating the integrity of the perforated patch. (Ac) After spontaneous break through, the dye diffuses into the cell body.

(B) Left traces, perforated-patch recordings of evoked IPSCs at varying holding potentials between −90 and −30 mV from the BC shown in (A). Middle and right traces, IPSCs recorded in the whole-cell configuration after break through at −70 mV in control conditions (middle) and in the presence of bicuculline (20 μM; right). Each trace is an average of 20 sweeps.

(C) Current-voltage relationship for the IPSCs shown in (B). Data points were fitted with a second-order polynomial function to determine E_{syn}. The interpolated reversal potential was −46 mV.

(D) Summary bar graph of E_{syn} values from BCs in rats and PV-BCs in transgenic mice.

(E) Summary bar graph of the corresponding resting membrane potentials. All BCs and PV-BCs had a fast-spiking phenotype; for BCs, the mean action-potential frequency tested with 1 s, 1 nA current pulses was 76.4 ± 3.4 Hz and the threshold was −38.1 ± 1.7 mV. Error bars in (D) and (E) indicate SEM.

corresponding to the high-coherence ($\kappa \geq 0.15$) region of the plot covered a broad range (12–90 Hz) (Figure 3A, color code). In contrast, the network based on shunting inhibition showed several differences in oscillatory properties. First, the coherence was selectively enhanced for low values of excitatory drive (Figure 3B). Second, although the high-coherence region had a comparable extent, it was shifted to higher g_{syn} values ($0.001\ mS\ cm^{-2} < g_{syn} < 0.1\ mS\ cm^{-2}$ for hyperpolarizing inhibition versus $0.01\ mS\ cm^{-2} < g_{syn} < 1\ mS\ cm^{-2}$ for shunting inhibition; Figures 3A and 3B). Finally, frequencies corresponding to the high-coherence region were narrowed to the upper γ band (50–90 Hz) (Figure 3B, color code). In conclusion, shunting inhibition enhances coherence at low excitation levels and helps to tune the network to γ frequencies.

To test whether our results were affected by details of the implementation of the network, we performed several control simulations. First, simulations were repeated after replacement of the Na^+ and K^+ channel models of Wang-Buzsáki by those of Erisir et al. (1999) (Figure S1). Second, simulations were performed for networks of different size (600 versus 200 neurons; Figures S2A and S2B) and for networks with different conduction delays (Figures S2C and S2D). Third, simulations were rerun with Poisson trains of fast excitatory synaptic conductances (Geiger et al., 1997) instead of tonic excitatory currents, with heterogeneous synaptic strength, and in the absence of gap junctions (Figures S2E–S2G). Under all conditions, the plots of κ versus I_μ and g_{syn} showed similar shape, suggesting that our conclusions can be generalized to a large range of network parameters.

Shunting Inhibition Improves Robustness of Gamma Oscillations against Heterogeneities

Shunting inhibition increases coherence in the presence of a low and moderately heterogeneous excitatory drive (Figure 3B). Does this reflect an increased robustness of oscillations against heterogeneity? To address this question, we increased the heterogeneity of the tonic excitatory drive to 35% (van Hooft et al., 2000) (Figures 3C and 3D). At this increased level of heterogeneity, coherent oscillations were abolished with hyperpolarizing inhibition (Figure 3C) but largely persisted with shunting inhibition (Figure 3D). Next, we systematically explored the effects of heterogeneity by varying the coefficient of variation of the tonic excitatory drive (I_σ/I_μ) between 0% and 100%. Figure 4 shows plots of coherence and frequency against I_σ/I_μ and g_{syn} for hyperpolarizing versus shunting inhibition (E_{syn} = −75 mV versus −55 mV) and weak ($0.5\ \mu A\ cm^{-2}$) versus strong ($3\ \mu A\ cm^{-2}$) tonic excitatory drive. In all scenarios coherence decreased with increasing heterogeneity (Wang and Buzsáki, 1996; Bartos et al., 2001). However, a large quantitative difference was apparent between hyperpolarizing and shunting inhibition. For the low excitatory drive, coherent oscillations ($\kappa \geq 0.15$) were generated for heterogeneity levels below 17% in a network based on hyperpolarizing inhibition (Figure 4A), whereas the critical value of heterogeneity was markedly higher (72%) in a network with shunting inhibition (Figure 4B). For the large excitatory drive, a similar albeit less pronounced enhancement of robustness of the oscillations was observed (critical values of heterogeneity 20% for hyperpolarizing inhibition and 32% for shunting inhibition; Figures 4C and 4D). Thus, shunting inhibition markedly increased the robustness of network oscillations against heterogeneity in the tonic excitatory drive.

Shunting Inhibition Increases Robustness of Gamma Oscillations by Homogenizing Single-Cell Firing Rates

How does shunting inhibition increase the robustness of γ oscillations in interneuron networks? To analyze the

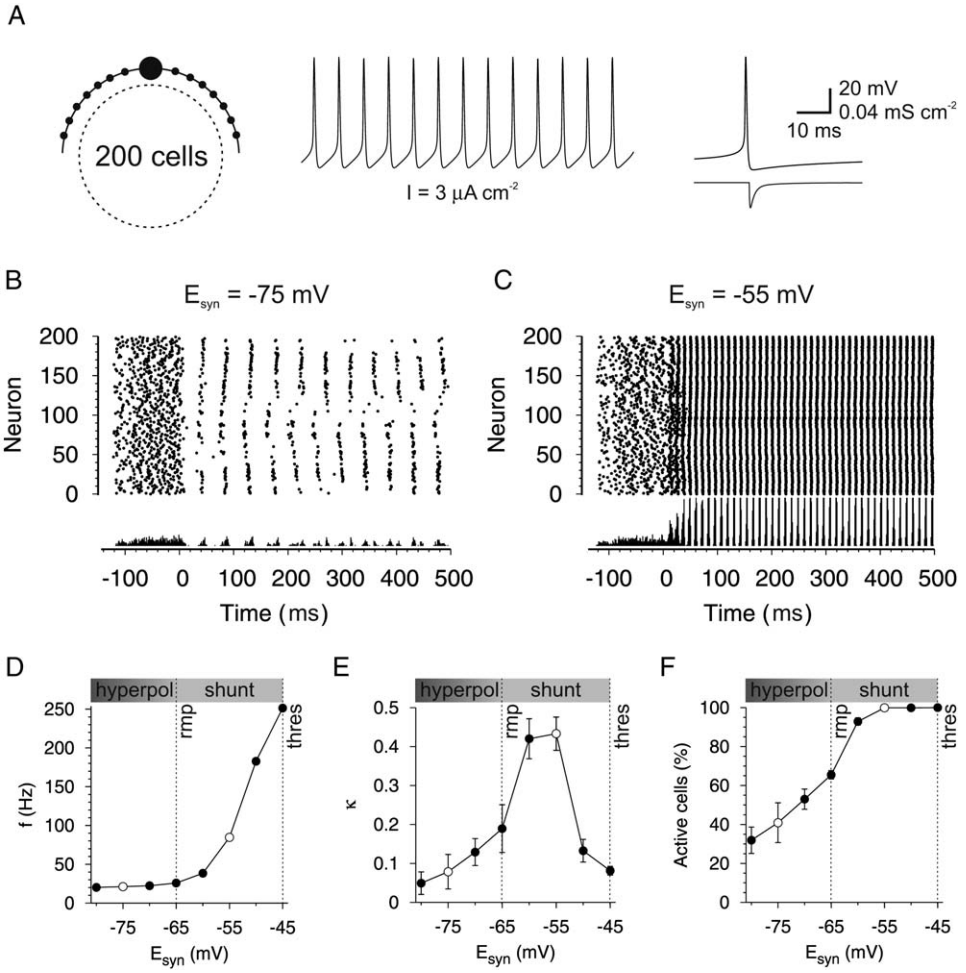

Figure 2. An Interneuron Network Model Based on Shunting Inhibition Generates Gamma Oscillations with High Coherence

(A) 200 single-compartment interneurons were arranged on a virtual ring. Each neuron was randomly connected, on average, to 57 of 100 neighboring cells by inhibitory synapses (left). Wang-Buzsáki conductances were inserted into the neurons to reproduce the fast-spiking action-potential phenotype of hippocampal BCs (middle). An action potential in a presynaptic neuron evokes a unitary inhibitory conductance in a postsynaptic neuron (g_{syn} = 0.04 mS cm^{-2}; right).

(B and C) Raster plots (top) and histograms of spike times (bottom; 1 ms bin width) of an interneuron network with default parameter settings for a hyperpolarized (E_{syn} = −75 mV [B]) and a depolarized reversal potential (E_{syn} = −55 mV [C]). The tonic excitatory drive had a mean amplitude (I_μ) of 0.5 μA cm^{-2} with a heterogeneity (I_σ / I_μ) of 10%. Synapses were activated at 0 ms.

(D–F) Network frequency (*f* [D]), coherence (κ [E]), and fraction of active neurons (F) are plotted against the reversal potential of the inhibitory conductance (E_{syn}). Each point represents mean ± standard deviation of five simulations. Open circles indicate the parameter settings used in the simulations shown in (B) and (C). Vertical dotted lines denote the resting membrane potential (−65 mV, rmp) and the approximate action-potential threshold (−45 mV, thres) of the model interneurons.

mechanisms underlying the complex effects of shunting inhibition, we simulated compound postsynaptic conductances in single neurons subjected to different excitation levels (Figure 5). Time course and amplitude of the conductance were obtained by convolution of the unitary postsynaptic conductance with the latency distribution, multiplied by the average number of presynaptic neurons. Thus, the applied compound conductance corresponded to the average inhibitory signal in a single cell of the fully synchronized network. With hyperpolarizing inhibition, the compound conductance prolonged the interspike intervals, independent of the excitation level (Figure 5A). In contrast, the effect of shunting inhibition was differential (see Stiefel et al. [2005]), depending on the excitation level in the simulated neuron. For low excitation levels, the interspike interval was reduced, whereas for high excitation levels the interval was increased (Figure 5B). The shortening of the interspike interval for low drive is explained by the depolarizing effect of the synaptic conductance, which sets the membrane to a subthreshold potential. Thus, the neuron is in a "ready-to-fire" mode, from which the next action potential can be generated as the synaptic conductance decays (Figure 5B). In contrast, the prolongation of the interspike interval for high drive is explained by the shunting effect of the synaptic conductance. Hence, shunting inhibition has a differential effect on weakly and strongly excited cells.

We further analyzed this differential effect by plotting the instantaneous action-potential frequency in the simulated cell against the tonic excitatory drive *I* for different values of g_{syn} (Figures 5C and 5D). For hyperpolarizing

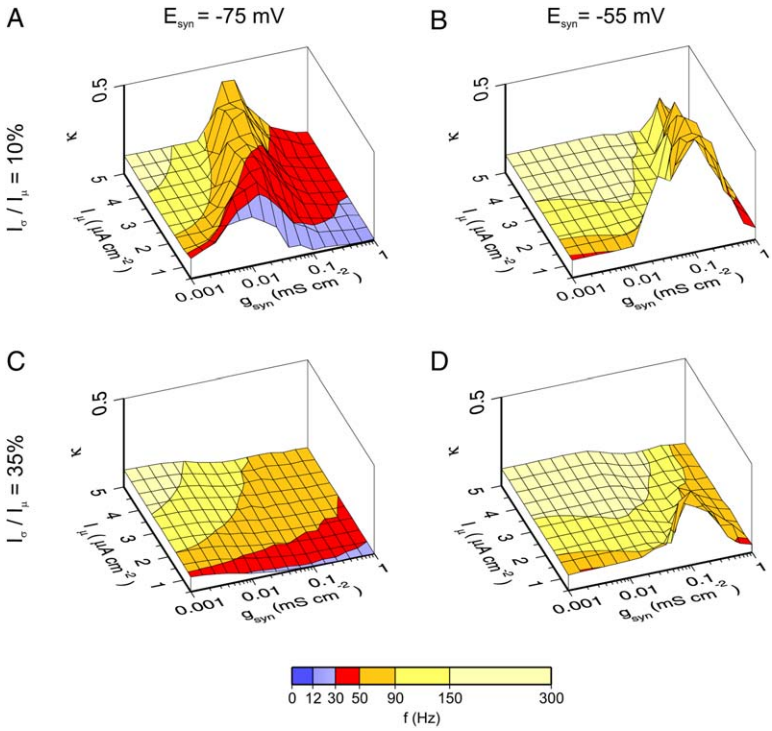

Figure 3. Shunting Inhibition Increases Coherence of Gamma Oscillations for Low Tonic Excitatory Drive

(A and B) Network coherence (κ) and frequency (*f*, superimposed color code) are plotted against amplitude of the tonic excitatory drive (I_μ) and peak unitary postsynaptic conductance (g_{syn}) for hyperpolarizing (E_{syn} = −75 mV [A]) and shunting inhibition (E_{syn} = −55 mV [B]). Heterogeneity (I_σ/I_μ) was 10%.

(C and D) Similar plots for increased heterogeneity in the tonic excitatory drive (I_σ/I_μ= 35%).

inhibition, the compound synaptic conductance reduced the maximal spike frequency of the simulated cell but did not change the shape of the *f-I* relation (Figure 5C). In contrast, for shunting inhibition, the synaptic conductance increased the frequency for low excitatory drive but decreased the frequency for high drive, reducing the slope of the *f-I* relation at suprathreshold values of *I* (Figure 5D). In a network of cells exposed to a heterogeneous tonic excitatory drive, the reduction in the slope of the *f-I* relation of single neurons will reduce the dispersion of action-potential frequencies. This homogenizing effect of shunting inhibition in single cells

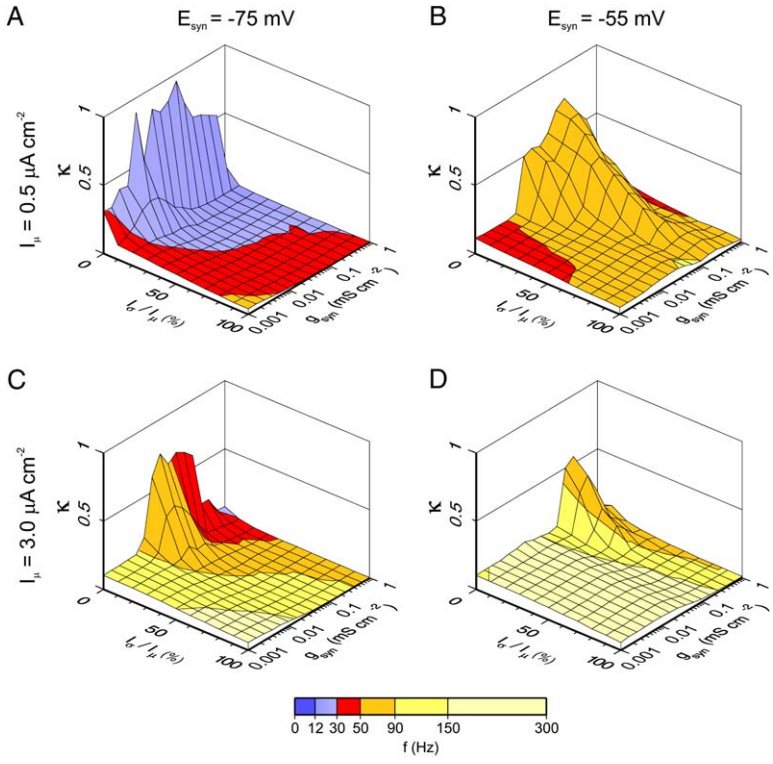

Figure 4. Shunting Inhibition Increases the Robustness against Heterogeneity of the Tonic Excitatory Drive

(A and B) Network coherence (κ) and frequency (*f*, color code) are plotted against the coefficient of variation of the excitatory drive (I_σ/I_μ) and the unitary postsynaptic peak conductance (g_{syn}) with hyperpolarizing (E_{syn} = −75 mV [A]) and shunting inhibition (E_{syn} = −55 mV [B]) for a small excitatory drive (I_μ= 0.5 μA cm^{-2}).

(C and D) Similar plots for a large excitatory drive (I_μ= 3.0 μA cm^{-2}).

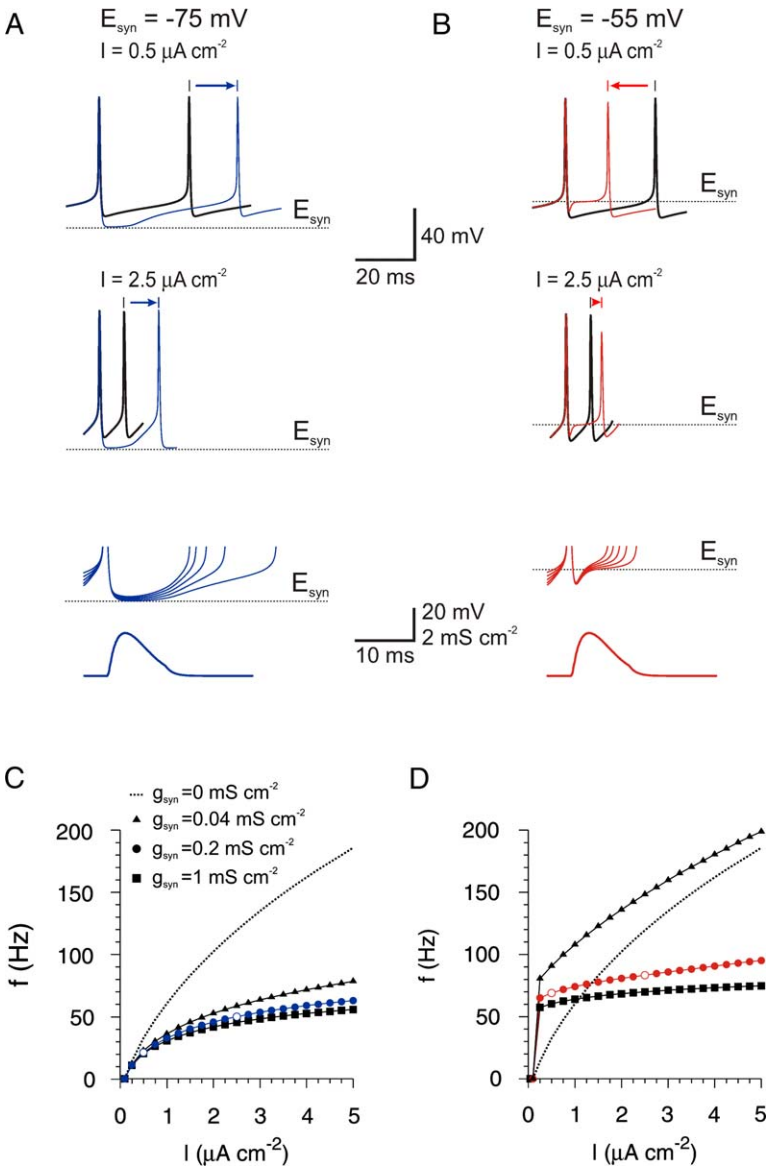

Figure 5. Shunting Inhibition Homogenizes Firing Frequencies in a Single-Cell Model

(A and B) Voltage traces from a single neuron without (black) and with a compound synaptic conductance (blue or red) triggered by the first action potential for low and high excitation levels (I = 0.5 μA cm^{-2}, top and I = 2.5 μA cm^{-2}, middle). Horizontal dotted lines indicate E_{syn}. Hyperpolarizing inhibition (E_{syn} = −75 mV) (A, blue traces) delays the onset of action potentials at both excitation levels (blue arrows). Shunting inhibition (E_{syn} = −55 mV) (B, red traces) leads to shortening of the interspike interval at low excitation levels (top, red arrow) but prolongation at high excitation levels (middle). The peak amplitude of the compound conductance was of 2.7 mS cm^{-2}, corresponding to a unitary g_{syn} of 0.2 mS cm^{-2}. Lower panels in (A) and (B) show superimposed voltage trajectories for I = 5, 4, 3, 2, and 1 μA cm^{-2} (left to right) and corresponding compound conductance at expanded time scale. Action potentials are shown truncated for clarity.

(C and D) Shunting inhibition changes the shape of input-output curves. Firing frequency (f) of the simulated neuron plotted against the amplitude of the tonic excitatory drive for hyperpolarizing (C) and shunting inhibition (D). g_{syn} was set to 0, 0.04, 0.2, and 1 mS cm^{-2}. f was calculated as the inverse of the interspike interval. Open circles in (C) and (D) correspond to the traces in (A) and (B).

(Figure 5D) explains the increased robustness of coherent oscillations against heterogeneities in the network (Figures 3 and 4).

Homogenization of Firing Frequencies by Artificial Shunting Conductances Added to Basket Cells with Dynamic Clamp

Unlike the model neurons used in the simulations, real neurons have complex morphology and express a variety of voltage-gated ion channels. To test whether the mechanisms of shunting inhibition also hold in real cells, we applied artificial inhibitory conductances to dentate gyrus BCs by a dynamic clamp (Figure 6). As in the single-cell simulations, the compound inhibitory conductance was obtained by convolution of unitary conductance and latency distribution in the model. Hyperpolarizing compound conductances triggered by single action potentials delayed the initiation of subsequent action potentials at both low and high excitation levels (Figures 6B and 6C, blue traces). In contrast, shunting compound conductances advanced action-potential initiation for low excitation levels but delayed spike initiation for high excitation levels (Figures 6B and 6C, red traces). For low excitatory drive, shunting compound conductances increased the instantaneous action-potential frequency from 40.6 ± 3.1 Hz to 46.2 ± 2.5 Hz ($p < 0.02$; seven cells; Figure 6D). In contrast, for high excitatory drive, shunting compound conductances reduced the discharge frequency from 99.4 ± 2.0 Hz to 66.7 ± 1.5 Hz ($p < 0.001$; Figure 6E). Thus, shunting inhibition added by dynamic clamp had a homogenizing effect on action-potential frequency in dentate gyrus BCs (Figure 6), closely reproducing the effect of shunting inhibition in the single-cell model (Figure 5).

Discussion

Our combined experimental and computational study revealed three major findings. First, the reversal potential of $GABA_A$ receptor-mediated synaptic currents in

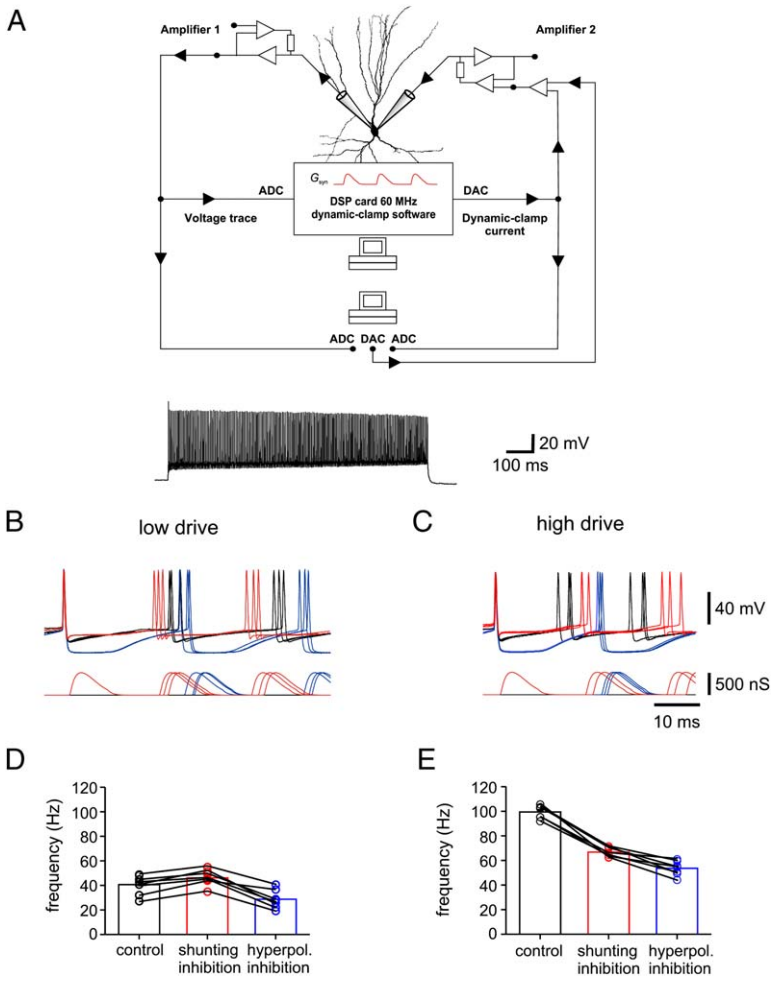

Figure 6. Homogenization of Firing Frequency in Hippocampal Basket Cells by Artificial Shunting Conductances

(A) Schematic illustration of the two-pipette dynamic-clamp configuration with a voltage recording (left) and a current-feeding pipette (right). Action potentials in the recorded neuron were used to trigger artificial compound inhibitory synaptic conductances (G_{syn}, inset). The dynamic-clamp current was calculated in real time from conductance, voltage, and assumed reversal potential (E_{syn}) and injected into the BC via amplifier 2. For details see Experimental Procedures. Lower trace shows fast-spiking action-potential phenotype.

(B and C) Differential effects of shunting (E_{syn} = −50 mV) and hyperpolarizing inhibition (E_{syn} = −75 mV) on action-potential frequency in a dentate gyrus BC with an excitatory drive of 230 pA (B) and 280 pA (C). Upper traces, superimposed action potentials recorded in the BC without inhibitory conductance (black), with shunting inhibition (red) and with hyperpolarizing inhibition (blue). Traces were temporally aligned to the first action potential. Lower trace, corresponding artificial conductances (520 nS peak amplitude). All data are from the same cell.

(D and E) Instantaneous action-potential frequency in BCs under control conditions, with shunting inhibition and with hyperpolarizing inhibition at low (D) and high excitation levels (E). Bars represent means, circles single-cell data (data from the same experiment are connected by lines). Error bars indicate SEM.

hippocampal BCs is between resting potential and action-potential threshold. We refer to this form of inhibition as "shunting." Second, when shunting inhibition is incorporated into an interneuron network model with realistic synaptic properties, coherent oscillations emerge. Finally, shunting inhibition introduces several functional advantages. In particular, it increases the robustness of the γ oscillator against heterogeneity in tonic excitatory drive and intrinsic firing frequency, offering a solution to a major weakness of previous interneuron network models. The principles identified here for isolated interneuron networks will also bear relevance to the oscillatory properties of mixed networks of interneurons and principal cells (Brunel and Wang, 2003), especially under conditions when principal cell activity is low (Jung and McNaughton, 1993).

Shunting Inhibition in Hippocampal Interneurons and Its Mechanisms

Our experimental findings indicate that $GABA_A$ receptor-mediated inhibition in fast-spiking, parvalbumin-expressing BCs is shunting rather than hyperpolarizing (Lamsa and Taira, 2003) or suprathreshold depolarizing (Ben-Ari, 2002). Similar results were previously obtained in interneurons of the amygdala and the cerebellum (Martina et al., 2001; Chavas and Marty, 2003), suggesting that shunting inhibition is a general principle of interneuron-interneuron signaling. What are the mechanisms underlying this relatively positive E_{syn}? In the simplest scenario, Cl^- ions would be passively distributed, and E_{syn} would be determined by the bicarbonate permeability of $GABA_A$ receptors (Kaila, 1994). For a Cl^- gradient corresponding to the mean resting potential of −58 mV in BCs and a bicarbonate-to-Cl^- permeability ratio of $GABA_A$ receptor channels of 0.18 to 0.33 (Bormann et al., 1987; Kaila, 1994), the estimated E_{syn} would be between −55 mV and −52 mV. Thus, the measured E_{syn} (−52.3 mV) in BCs is consistent with a simple scenario in which Cl^- is distributed passively.

Intracellular Cl^- concentration, and therefore E_{syn}, will also depend on the activity of transporters, such as the K^+/Cl^- cotransporter KCC, which mediates Cl^- extrusion, and the $Na^+/K^+/Cl^-$ cotransporter NKCC, which mediates Cl^- uptake. Immunocytochemical studies suggested a substantial expression of KCC2 in parvalbumin-positive interneurons (Gulyás et al., 2001). KCC2 would be expected to generate a more negative E_{syn} (Kaila, 1994; Payne et al., 2003), in apparent contrast to the experimental observations. Thus, our results may suggest that the activity of KCC2 is downregulated in BCs (see Woodin et al. [2003]). Alternatively, Cl^- extrusion by KCCs may be counterbalanced by uptake

through NKCCs, or by influx through Cl^- channels (Jentsch et al., 2002).

Shunting Inhibition Promotes Coherent Oscillatory Activity in Interneuron Networks with Realistic Synaptic Properties

Our computational analysis revealed that shunting inhibition can support coherent oscillations in interneuron networks. This is unexpected because previous modeling studies demonstrated that coherent oscillations break down if the synaptic reversal potential is more positive than the afterhyperpolarization after an action potential (van Vreeswijk et al., 1994; Wang and Buzsáki, 1996). How is it possible that in our network model, oscillations are paradoxically supported by shunting inhibition? In previous interneuron network models without synaptic latencies, coherent γ oscillations are generated with weak, slow, and hyperpolarizing synapses. If one of these synaptic parameters is changed, coherence is abolished (Wang and Buzsáki, 1996; I.V. and P.J., unpublished data). However, two additional aspects have to be considered. First, introducing synaptic delays increases coherence under various conditions (Bartos et al., 2002; Maex and de Schutter, 2003; Brunel and Wang, 2003). Second, the combined change of synaptic factors gives unexpected improvements of coherence. In particular, the combination of strong and fast synapses is a highly efficient synchronization signal (Bartos et al., 2002). In a network based on these synaptic properties, both hyperpolarizing and shunting inhibition can lead to highly coherent oscillations (Figure 3).

A network based on shunting inhibition requires large unitary g_{syn} or, equivalently, a high synaptic connectivity to generate a sufficiently large compound conductance. In our network, in which a neuron on average receives input from 57 other cells (Sik et al., 1995), the g_{syn} values necessary for coherent oscillations are compatible with the upper range of experimental observations (Bartos et al., 2002) (Experimental Procedures). However, if synaptic connectivity is higher (Gulyás et al., 1999), the requirement for a high g_{syn} would be reduced. Thus, an interneuron network combining synaptic latencies, strong and fast synapses, and shunting inhibition is a highly plausible γ oscillator.

Functional Advantages Introduced by Shunting Inhibition

Shunting inhibition not only supports coherent γ oscillations but unexpectedly adds several advantages to interneuron network function. Most importantly, this form of inhibition greatly relaxes the requirements for amplitude and heterogeneity of the tonic excitatory drive. First, whereas interneuron networks with hyperpolarizing inhibition require a tonic excitatory drive of $\sim 3\ \mu A\ cm^{-2}$, networks with shunting inhibition produce coherent γ oscillations with a drive of $\sim 0.5\ \mu A\ cm^{-2}$ (Figure 3). The latter value is more consistent with experimental data on tonic excitatory currents in fast-spiking interneurons (60 pA/12000 μm^2 = 0.5 $\mu A\ cm^{-2}$ for mGluR responses [van Hooft et al., 2000]; 51 pA/12000 μm^2 = 0.4 $\mu A\ cm^{-2}$ for kainate responses [Fisahn et al., 2004]; in which 12000 μm^2 is the approximate somatodendritic surface area of BCs [Bartos et al., 2001]). Second, although networks based on hyperpolarizing inhibition tolerate heterogeneity levels between ~3% and 10%, our model based on shunting inhibition robustly generates coherent oscillations with heterogeneity levels up to ~70%. Again, the latter value is more consistent with experimental data on the coefficient of variation of tonic currents in fast-spiking interneurons (~35% for mGluR responses [van Hooft et al., 2000]; ~53% for kainate responses [Fisahn et al., 2004]).

Finally, shunting inhibition also confers advantages in frequency control. Within a given network, shunting inhibition increases the precision of frequency tuning, making network frequency relatively independent of tonic excitatory drive and synaptic conductance (Figure 3B). However, shunting inhibition still permits the regulation of network frequency by other factors, such as properties of active conductances (Jonas et al., 2004) (Figure S1) and synaptic latencies (Bartos et al., 2002; Maex and de Schutter, 2003; Brunel and Wang, 2003) (Figures S2C and S2D). The properties of active conductances could be regulated, in turn, by differential expression or phosphorylation of Kv3 subunits in interneurons (Rudy and McBain, 2001; Lien and Jonas, 2003). The synaptic latencies will depend on the structure of the network (small versus large) and the spatial distribution of the activating stimuli (focal versus global) (Bartos et al., 2002). Although the precise connectivity pattern is unknown, different frequencies of γ oscillations in the dentate gyrus (40–100 Hz) and the CA3/CA1 regions (25–50 Hz) (Bragin et al., 1995; Towers et al., 2002; Whittington et al., 1995) may be interpreted as differences in network structure (Figures S2C and S2D).

How Does Shunting Inhibition Promote Coherent Gamma Activity?

Although hyperpolarizing conductances have consistent inhibitory effects on neuronal activity, shunting conductances can have both inhibitory and excitatory actions (Alger and Nicoll, 1979; Andersen et al., 1980; Chavas and Marty, 2003; Gulledge and Stuart, 2003; Stiefel et al., 2005). If E_{syn} is between resting potential and action-potential threshold, the effect of the $GABA_A$ receptor-mediated conductance consists of two temporal phases (Stein and Nicoll, 2003; Gulledge and Stuart, 2003). This is observed in both our single-cell models (Figure 5) and the dynamic-clamp experiments (Figure 6). In the first phase, the conductance increase leads to a reduction in the excitability of the cell, despite the concurrent depolarization. The membrane is held at a subthreshold potential near E_{syn}, and the cell cannot fire. In the second phase, when the conductance has decayed but the membrane depolarization persists, excitability is increased. Thus, an action potential can be initiated with short delay in the presence of a tonic excitatory drive.

The biphasic effect of shunting inhibition explains its differential, excitation level-dependent action (Figures 5 and 6). For high excitation levels the first inhibitory phase will dominate, shifting the subsequent action potential to later times. In contrast, for low excitation levels, the second excitatory phase will be relevant, advancing the next action potential in comparison to control conditions. Thus, in a scenario with tonic drive, shunting inhibition has excitation level-dependent effects on action-potential timing, resembling a recently reported

scenario with fluctuating drive in which shunting inhibition has phase-dependent effects (Stiefel et al., 2005). As a consequence, at the single-cell level, the action-potential frequency becomes relatively independent of the tonic excitatory drive. At the network level, action-potential frequencies are homogenized, which counterbalances the effects of heterogeneity in the tonic excitatory drive. Therefore, the basic properties of shunting inhibition explain the greater robustness of network oscillations against heterogeneities.

In summary, we have shown that inhibition in hippocampal interneurons is shunting and that interneuron networks based on strong, fast, and shunting synapses are highly efficient γ oscillators. Thus, our findings may explain the remarkable robustness of γ oscillations observed in vitro (Whittington et al., 1995; Towers et al., 2002; Fisahn et al., 2004; Hájos et al., 2004; Gloveli et al., 2005) and in vivo (Bragin et al., 1995; Csicsvari et al., 2003). Given the striking similarities of mutual inhibition across regions (Martina et al., 2001; Chavas and Marty, 2003; Galarreta and Hestrin, 2002; Bartos et al., 2002; this paper), our results may define a universal mechanism of oscillatory activity in the brain.

Experimental Procedures

Perforated-Patch Recording

Transverse 300 μm thick hippocampal slices were cut from brains of 19- to 25-day-old Wistar rats with a Dosaka DTK-1000 vibratome. In a subset of experiments, transgenic mice (C57/Bl6) expressing the enhanced green fluorescent protein (EGFP) under the control of the parvalbumin promoter were used, in which parvalbumin-containing BCs are selectively labeled (Bartos et al., 2002; Meyer et al., 2002). Animals were handled in accordance with national and institutional guidelines. Slices were superfused with physiological extracellular solution containing 125 mM NaCl, 25 mM $NaHCO_3$, 25 mM glucose, 2.5 mM KCl, 1.25 mM NaH_2PO_4, 2 mM $CaCl_2$, and 1 mM $MgCl_2$ (equilibrated with 95% O_2/5% CO_2 gas mixture). To isolate $GABA_A$ receptor-mediated synaptic currents, we added 10 μM 6-cyano-7-nitroquinoxaline-2,3-dione (CNQX, Tocris), 50 μM D-2-amino-5-phosphonopentanoic acid (D-AP5, Tocris), and 1 μM CGP55845A (Tocris). To verify that IPSCs were mediated by $GABA_A$ receptors, we further added bicuculline methiodide (Sigma) in a subset of experiments. Recordings were made under visual control by infrared-differential interference contrast (IR-DIC) videomicroscopy. For perforated-patch recordings, pipettes (borosilicate glass tubing, 2 mm outer diameter, 1 mm wall thickness) were tip filled with a solution containing 78 mM KCl, 78 mM K-gluconate, 5 mM $MgCl_2$, 10 mM HEPES, 5 mM glucose (pH 7.2) (KOH, 308–315 mOsm) and back filled with the same solution further containing gramicidin D (10–20 μg/ml, Sigma), Alexa 594 (50–100 μM, Molecular Probes), and biocytin (0.5–1 mg/ml, Molecular Probes). Pipette resistance was 2.5–4 MΩ. To ensure the integrity of the perforated-patch configuration, we examined cells with epifluorescence illumination at ~1 min intervals. A transition from perforated-patch to whole-cell configuration was indicated by a fluorescent labeling of the cell body and a sudden depolarizing shift in the IPSC reversal potential.

Pipettes used for stimulation of presynaptic axons were filled with HEPES-buffered Na^+-rich solution (pH 7.4) and placed in the granule cell layer. Single electrical stimuli (intensity 5–40 V, duration 0.1–0.2 ms) were applied at a frequency of 0.2 Hz. IPSCs were recorded with an Axopatch 200B amplifier; the holding potentials were set to values between −100 and −30 mV. Series resistance (R_S) was 80–100 MΩ and compensated by 65%–75% (lag 40–60 μs). IPSCs were low-pass filtered at 5 kHz and digitized at 10 kHz with a CED 1401plus laboratory interface connected to a Pentium PC. Igor-based programs (FPulse; homemade) were used for stimulus generation and data acquisition. Resting potential was measured in the track mode of the Axopatch amplifier. Interneurons recorded had somata located at the granule cell layer-hilus border. BCs in rat slices were identified by their fast-spiking action-potential phenotype and the location of the axon in the granule cell layer (Buhl et al., 1994) in posthoc morphological analysis. EGFP-expressing BCs were visually identified by epifluorescence illumination (Bartos et al., 2002). Spiking patterns were tested immediately after breaking through the membrane with 1 s, 1 nA depolarizing pulses; action-potential threshold was determined as the voltage at which the rate of rise first exceeded 20 mV ms^{-1}. For morphological analysis, biocytin-filled neurons were visualized with avidin-biotinylated peroxidase complex and 3,3′-diaminobenzidine as chromogen (Bartos et al., 2001). Recording temperature was 22ºC–24ºC.

Evoked IPSCs were averaged from 10–30 single traces at each holding potential. The mean peak amplitude of IPSCs was measured from the preceding baseline and plotted against holding potential. Data points in the resulting current-voltage (*I-V*) relations were fitted with a second order polynomial function to determine the reversal potential of synaptically evoked IPSCs (E_{syn}). Membrane potentials and E_{syn} are reported without correction for the liquid junction potential.

Structure of Interneuron Network Model

The activity of a network of fast-spiking inhibitory interneurons was simulated with Neuron 5.5 running on an Pentium PC under Linux (Hines and Carnevale, 1997). In the standard model, neurons were represented as single compartments with a specific leak conductance of 0.1 mS cm^{-2}. Voltage-gated Na^+ and K^+ conductances were modeled according to Wang and Buzsáki (1996). Properties of model synapses were based on experimental paired recording data (Bartos et al., 2002). The rise-time constant of the synaptic conductance was assumed as 0.16 ms, and the decay-time constants were set to 1.2 ms (90% amplitude contribution) and 8 ms (10%). Recordings in the three hippocampal subfields revealed a unitary inhibitory conductance change with mean peak amplitudes of 2.5–6.1 nS. Thus, estimated specific conductances (conductance per membrane surface area) are 0.02–0.05 mS cm^{-2} if related to the total surface area of soma and dendrites (~12000 μm^2) (Bartos et al., 2001) and 0.2–0.5 mS cm^{-2} if related to the area of the soma only (~1300 μm^2). In the simulations, the unitary postsynaptic peak conductance (g_{syn}) was varied from 0.001 to 1 mS cm^{-2} to fully cover this range. E_{syn} was varied between −80 and −45 mV.

The interneuron network model was assembled from 200 neurons arranged on a virtual ring with 50 μm spacing between adjacent cells (Bartos et al., 2002). Each neuron was randomly connected to a subpopulation of its 100 nearest neighbors by inhibitory synapses with a probability of 0.57. Although the exact pattern of interneuron connectivity is unknown, these assumptions are consistent with anatomical data on the numbers of synaptic connections among parvalbumin-positive interneurons in CA1 (Sik et al., 1995; Gulyás et al., 1999). The synaptic latency of the postsynaptic conductance consisted of a constant synaptic delay (0.5 ms) and a variable conduction delay (0–10 ms), calculated from the distance between pre- and postsynaptic cells along the circumference of the ring (conduction velocity 0.25 m s^{-1}). Additionally, each neuron was randomly connected to four of its eight nearest neighbors by electrical synapses (transcellular conductance 0.01 mS cm^{-2}) (Traub et al., 2001; Bartos et al., 2002).

Network Simulations

Neurons were initialized to a resting membrane potential of −65 mV, and activity was initiated by applying tonic excitatory currents to the neurons with amplitudes randomly chosen from a normal distribution (with mean I_μ and standard deviation I_σ). I_μ ranged from 0.25–5 μA cm^{-2}. I_σ/I_μ was typically 10%; in a subset of simulations, it was varied between 0% and 100%. To examine the emergence of synchronization from a disordered initial condition, we applied driving currents to individual neurons with randomized onset times taken from a uniform distribution in the range $-150\ ms \leq t < -100\ ms$. Chemical and electrical synapses were inactive at $-150\ ms \leq t < 0$ and enabled at $t = 0$. In all simulations, the time step was 10 μs.

Coherence of network activity was analyzed in 100 ms epochs ($400\ ms \leq t < 500\ ms$). Frequency was determined in 200 ms epochs ($300\ ms \leq t < 500\ ms$) to increase the accuracy at low frequencies. The time of an action potential was determined as the first point in

the rising phase that exceeded 0 mV. Frequency (f) was determined as the mean of the inverse of the interspike intervals. Coherence (κ), a measure for network synchrony, was determined by binning action-potential time points at 0.1 / f intervals and calculating a cross correlation-based index (Wang and Buzsáki, 1996). Frequency and coherence values given in the figures are means of five simulations with initial conditions randomized for each run.

For all simulations shown in the figures, the standard model (see above) was used. In a subset of simulations shown in the supplemental figures, different active conductances and different values of network size, connectivity, and conduction delays were assumed, as indicated explicitly. In additional simulations (Figure S2E), phasic instead of tonic excitatory drive was used. Finally, in a subset of simulations heterogeneity in g_{syn} was introduced or gap junctions were omitted.

Single-Cell Simulations and Spike-Triggered Dynamic Clamp

To examine the effects of compound synaptic conductances on the interspike interval at the single-neuron level, we convolved the unitary synaptic conductance with the latency distribution point by point and multiplied with the average number of connected neurons (57 cells). The compound synaptic conductance was then added to a single neuron subjected to a tonic excitatory drive, at a time point defined by the first action potential occurring > 300 ms after current injection.

To test the effects of compound synaptic conductances in real interneurons, we added artificial conductances to dentate gyrus BCs by the dynamic clamp technique, as described previously (Lien and Jonas, 2003; see Prinz et al. [2004]). Experiments were made in either a single- or a double-electrode configuration (three and four cells, respectively). As the results were independent of the configuration, data were pooled. Pipettes were filled with a solution containing 40 mM KCl, 110 mM K-gluconate, 0.1 mM EGTA, 2 mM $MgCl_2$, 2 mM Na_2ATP, 10 mM HEPES, and 0.5 mg/ml biocytin (pH 7.2) (KOH). For dynamic clamp experiments, the recording temperature was 32ºC–34ºC.

The hardware of the system was based on a digital signal processor (DSP) card (TMS320C32; Texas Instruments; supplied by Innovative Integration, Westlake Village, CA). The card was driven by homemade programs written in C and compiled with a Texas Instruments compiler running on the host PC. Computations were performed in real time, with an onboard timer and an interrupt-driven procedure. The throughput rate of the system was 80 kHz (Lien and Jonas, 2003). Membrane potential was low-pass filtered at 30 kHz and digitized by the ADC of the DSP card. When overshooting action potentials (V > 0 mV) occurred in the recorded neuron, an artificial inhibitory conductance was triggered. As in the single-neuron simulations (Figure 5), the average compound conductance from the fully synchronized network model was used. The compound conductance was specified at 100 μs resolution, and intermediate values were calculated by linear interpolation. Finally, the artificial synaptic current was calculated as $I(t) = g(t) \times [E_{syn} - V(t)]$, in which $g(t)$ is the compound conductance, E_{syn} the assumed reversal potential, and $V(t)$ the measured voltage of the neuron. For shunting inhibition, E_{syn} was assumed as −50 mV, to account for the ~5 mV more positive firing threshold (−40.6 ± 2.5 mV for recorded neurons [four cells at 33ºC] and −45.9 mV for model cells). To investigate the effects of inhibition, we evoked trains of action potentials in BCs by 1 s depolarizing current pulses of different amplitudes. To block spontaneous synaptic events, we performed these experiments in the presence of 10 μM CNQX and 20 μM bicuculline. Action-potential frequency was calculated as the mean of the inverse of >20 interspike intervals.

Statistics

Values are given as mean ± SEM. Statistical significance was assessed by two-sided nonparametric Kruskal-Wallis or Wilcoxon signed rank tests at the significance level (p) indicated.

Supplemental Data

The Supplemental Data for this article can be found online at http://www.neuron.org/cgi/content/full/49/1/107/DC1/.

Acknowledgments

We thank Drs. A. Aertsen, J. Bischofberger, G. Buzsáki, and M. Frotscher for critically reading the manuscript and Drs. A. Meyer and H. Monyer for kindly providing the transgenic mice. We also thank K. Winterhalter and U. Nöller for technical assistance and U. Fröbe for programming. This work was supported by grants of Deutsche Forschungsgemeinschaft (SFB 505/C6), Volkswagenstiftung (I/78563), and Bundesministerium für Bildung und Forschung (OI GQ 0420).

Received: August 12, 2005
Revised: October 12, 2005
Accepted: November 18, 2005
Published: January 4, 2006

References

Alger, B.E., and Nicoll, R.A. (1979). GABA-mediated biphasic inhibitory responses in hippocampus. Nature *281*, 315–317.

Andersen, P., Dingledine, R., Gjerstad, L., Langmoen, I.A., and Laursen, A.M. (1980). Two different responses of hippocampal pyramidal cells to application of gamma-amino butyric acid. J. Physiol. *305*, 279–296.

Bartos, M., Vida, I., Frotscher, M., Geiger, J.R.P., and Jonas, P. (2001). Rapid signaling at inhibitory synapses in a dentate gyrus interneuron network. J. Neurosci. *21*, 2687–2698.

Bartos, M., Vida, I., Frotscher, M., Meyer, A., Monyer, H., Geiger, J.R.P., and Jonas, P. (2002). Fast synaptic inhibition promotes synchronized gamma oscillations in hippocampal interneuron networks. Proc. Natl. Acad. Sci. USA *99*, 13222–13227.

Bazhenov, M., Timofeev, I., Steriade, M., and Sejnowski, T.J. (1999). Self-sustained rhythmic activity in the thalamic reticular nucleus mediated by depolarizing $GABA_A$ receptor potentials. Nat. Neurosci. *2*, 168–174.

Ben-Ari, Y. (2002). Excitatory actions of GABA during development: the nature of the nurture. Nat. Rev. Neurosci. *3*, 728–739.

Bormann, J., Hamill, O.P., and Sakmann, B. (1987). Mechanism of anion permeation through channels gated by glycine and γ-aminobutyric acid in mouse cultured spinal neurones. J. Physiol. *385*, 243–286.

Bragin, A., Jandó, G., Nádasdy, Z., Hetke, J., Wise, K., and Buzsáki, G. (1995). Gamma (40–100 Hz) oscillation in the hippocampus of the behaving rat. J. Neurosci. *15*, 47–60.

Brunel, N., and Wang, X.-J. (2003). What determines the frequency of fast network oscillations with irregular neural discharges? I. Synaptic dynamics and excitation-inhibition balance. J. Neurophysiol. *90*, 415–430.

Buhl, E.H., Halasy, K., and Somogyi, P. (1994). Diverse sources of hippocampal unitary inhibitory postsynaptic potentials and the number of synaptic release sites. Nature *368*, 823–828.

Buzsáki, G., and Draguhn, A. (2004). Neuronal oscillations in cortical networks. Science *304*, 1926–1929.

Chavas, J., and Marty, A. (2003). Coexistence of excitatory and inhibitory GABA synapses in the cerebellar interneuron network. J. Neurosci. *23*, 2019–2031.

Csicsvari, J., Jamieson, B., Wise, K.D., and Buzsáki, G. (2003). Mechanisms of gamma oscillations in the hippocampus of the behaving rat. Neuron *37*, 311–322.

Dan, Y., and Poo, M.-M. (2004). Spike timing-dependent plasticity of neural circuits. Neuron *44*, 23–30.

Erisir, A., Lau, D., Rudy, B., and Leonard, C.S. (1999). Function of specific K^+ channels in sustained high-frequency firing of fast-spiking neocortical interneurons. J. Neurophysiol. *82*, 2476–2489.

Ermentrout, G.B., and Kopell, N. (1990). Oscillator death in systems of coupled neural oscillators. SIAM J. Appl. Math. *50*, 125–146.

Fisahn, A., Contractor, A., Traub, R.D., Buhl, E.H., Heinemann, S.F., and McBain, C.J. (2004). Distinct roles for the kainate receptor subunits GluR5 and GluR6 in kainate-induced hippocampal gamma oscillations. J. Neurosci. *24*, 9658–9668.

Fricker, D., Verheugen, J.A., and Miles, R. (1999). Cell-attached measurements of the firing threshold of rat hippocampal neurones. J. Physiol. *517*, 791–804.

Galarreta, M., and Hestrin, S. (2002). Electrical and chemical synapses among parvalbumin fast-spiking GABAergic interneurons in adult mouse neocortex. Proc. Natl. Acad. Sci. USA *99*, 12438–12443.

Geiger, J.R.P., Lübke, J., Roth, A., Frotscher, M., and Jonas, P. (1997). Submillisecond AMPA receptor-mediated signaling at a principal neuron-interneuron synapse. Neuron *18*, 1009–1023.

Gloveli, T., Dugladze, T., Saha, S., Monyer, H., Heinemann, U., Traub, R.D., Whittington, M.A., and Buhl, E.H. (2005). Differential involvement of oriens/pyramidale interneurones in hippocampal network oscillations *in vitro*. J. Physiol. *562*, 131–147.

Gulledge, A.T., and Stuart, G.J. (2003). Excitatory actions of GABA in the cortex. Neuron *37*, 299–309.

Gulyás, A.I., Megías, M., Emri, Z., and Freund, T.F. (1999). Total number and ratio of excitatory and inhibitory synapses converging onto single interneurons of different types in the CA1 area of the rat hippocampus. J. Neurosci. *19*, 10082–10097.

Gulyás, A.I., Sik, A., Payne, J.A., Kaila, K., and Freund, T.F. (2001). The KCl cotransporter, KCC2, is highly expressed in the vicinity of excitatory synapses in the rat hippocampus. Eur. J. Neurosci. *13*, 2205–2217.

Hájos, N., Pálhalmi, J., Mann, E.O., Németh, B., Paulsen, O., and Freund, T.F. (2004). Spike timing of distinct types of GABAergic interneuron during hippocampal gamma oscillations *in vitro*. J. Neurosci. *24*, 9127–9137.

Hines, M.L., and Carnevale, N.T. (1997). The NEURON simulation environment. Neural Comput. *9*, 1179–1209.

Jentsch, T.J., Stein, V., Weinreich, F., and Zdebik, A.A. (2002). Molecular structure and physiological function of chloride channels. Physiol. Rev. *82*, 503–568.

Jonas, P., Bischofberger, J., Fricker, D., and Miles, R. (2004). Fast in, fast out—temporal and spatial signal processing in hippocampal interneurons. Trends Neurosci. *27*, 30–40.

Jung, M.W., and McNaughton, B.L. (1993). Spatial selectivity of unit activity in the hippocampal granular layer. Hippocampus *3*, 165–182.

Kaila, K. (1994). Ionic basis of $GABA_A$ receptor channel function in the nervous system. Prog. Neurobiol. *42*, 489–537.

Kopell, N., and Ermentrout, B. (2004). Chemical and electrical synapses perform complementary roles in the synchronization of interneuronal networks. Proc. Natl. Acad. Sci. USA *101*, 15482–15487.

Kyrozis, A., and Reichling, D.B. (1995). Perforated-patch recording with gramicidin avoids artifactual changes in intracellular chloride concentration. J. Neurosci. Methods *57*, 27–35.

Lamsa, K., and Taira, T. (2003). Use-dependent shift from inhibitory to excitatory $GABA_A$ receptor action in SP-O interneurons in the rat hippocampal CA3 area. J. Neurophysiol. *90*, 1983–1995.

Lien, C.C., and Jonas, P. (2003). Kv3 potassium conductance is necessary and kinetically optimized for high-frequency action potential generation in hippocampal interneurons. J. Neurosci. *23*, 2058–2068.

Lisman, J.E. (1999). Relating hippocampal circuitry to function: recall of memory sequences by reciprocal dentate-CA3 interactions. Neuron *22*, 233–242.

Maex, R., and de Schutter, E. (2003). Resonant synchronization in heterogeneous networks of inhibitory neurons. J. Neurosci. *23*, 10503–10514.

Martina, M., Royer, S., and Paré, D. (2001). Cell-type-specific GABA responses and chloride homeostasis in the cortex and amygdala. J. Neurophysiol. *86*, 2887–2895.

Meyer, A.H., Katona, I., Blatow, M., Rozov, A., and Monyer, H. (2002). *In vivo* labeling of parvalbumin-positive interneurons and analysis of electrical coupling in identified neurons. J. Neurosci. *22*, 7055–7064.

Neltner, L., Hansel, D., Mato, G., and Meunier, C. (2000). Synchrony in heterogeneous networks of spiking neurons. Neural Comput. *12*, 1607–1641.

Parra, P., Gulyás, A.I., and Miles, R. (1998). How many subtypes of inhibitory cells in the hippocampus? Neuron *20*, 983–993.

Payne, J.A., Rivera, C., Voipio, J., and Kaila, K. (2003). Cation-chloride co-transporters in neuronal communication, development and trauma. Trends Neurosci. *26*, 199–206.

Penttonen, M., Kamondi, A., Acsády, L., and Buzsáki, G. (1998). Gamma frequency oscillation in the hippocampus of the rat: intracellular analysis *in vivo*. Eur. J. Neurosci. *10*, 718–728.

Prinz, A.A., Abbott, L.F., and Marder, E. (2004). The dynamic clamp comes of age. Trends Neurosci. *27*, 218–224.

Rudy, B., and McBain, C.J. (2001). Kv3 channels: voltage-gated K^+ channels designed for high-frequency repetitive firing. Trends Neurosci. *24*, 517–526.

Salinas, E., and Sejnowski, T.J. (2001). Correlated neuronal activity and the flow of neural information. Nat. Rev. Neurosci. *2*, 539–550.

Sik, A., Penttonen, M., Ylinen, A., and Buzsáki, G. (1995). Hippocampal CA1 interneurons: an *in vivo* intracellular labeling study. J. Neurosci. *15*, 6651–6665.

Singer, W. (1999). Neuronal synchrony: a versatile code for the definition of relations? Neuron *24*, 49–65.

Stein, V., and Nicoll, R.A. (2003). GABA generates excitement. Neuron *37*, 375–378.

Stiefel, K.M., Wespatat, V., Gutkin, B., Tennigkeit, F., and Singer, W. (2005). Phase dependent sign changes of GABAergic synaptic input explored *in-silicio* and *in-vitro*. J. Comput. Neurosci. *19*, 71–85.

Tiesinga, P.H.E., and José, J.V. (2000). Robust gamma oscillations in networks of inhibitory hippocampal interneurons. Network *11*, 1–23.

Towers, S.K., LeBeau, F.E., Gloveli, T., Traub, R.D., Whittington, M.A., and Buhl, E.H. (2002). Fast network oscillations in the rat dentate gyrus in vitro. J. Neurophysiol. *87*, 1165–1168.

Traub, R.D., Whittington, M.A., Colling, S.B., Buzsáki, G., and Jefferys, J.G.R. (1996). Analysis of gamma rhythms in the rat hippocampus *in vitro* and *in vivo*. J. Physiol. *493*, 471–484.

Traub, R.D., Jefferys, J.G.R., and Whittington, M.A. (1999). Fast Oscillations in Cortical Circuits (Cambridge, MA: MIT Press).

Traub, R.D., Kopell, N., Bibbig, A., Buhl, E.H., LeBeau, F.E., and Whittington, M.A. (2001). Gap junctions between interneuron dendrites can enhance synchrony of gamma oscillations in distributed networks. J. Neurosci. *21*, 9478–9486.

van Hooft, J.A., Giuffrida, R., Blatow, M., and Monyer, H. (2000). Differential expression of group I metabotropic glutamate receptors in functionally distinct hippocampal interneurons. J. Neurosci. *20*, 3544–3551.

van Vreeswijk, C., Abbott, L.F., and Ermentrout, G.B. (1994). When inhibition not excitation synchronizes neural firing. J. Comput. Neurosci. *1*, 313–321.

Wang, X.-J., and Buzsáki, G. (1996). Gamma oscillation by synaptic inhibition in a hippocampal interneuronal network model. J. Neurosci. *16*, 6402–6413.

Wang, X.-J., and Rinzel, J. (1992). Alternating and synchronous rhythms in reciprocally inhibitory model neurons. Neural Comput. *4*, 84–97.

White, J.A., Chow, C.C., Ritt, J., Soto-Treviño, C., and Kopell, N. (1998). Synchronization and oscillatory dynamics in heterogeneous, mutually inhibited neurons. J. Comput. Neurosci. *5*, 5–16.

Whittington, M.A., Traub, R.D., and Jefferys, J.G.R. (1995). Synchronized oscillations in interneuron networks driven by metabotropic glutamate receptor activation. Nature *373*, 612–615.

Woodin, M.A., Ganguly, K., and Poo, M.-M. (2003). Coincident pre- and postsynaptic activity modifies GABAergic synapses by postsynaptic changes in Cl^- transporter activity. Neuron *39*, 807–820.